materials proceedings

MDPI

Proceeding Paper

Low-Cost Hydrothermally Synthesized Multifunctional Rare Earth Metal Yttrium Cerium Oxide †

Shivangi Srivastava * and Narendra Km. Pandey

Department of Physics, University of Lucknow; profnarendrapandey137@gmail.com

* Correspondence: shivangsrivastav007@gmail.com

† Presented at the 4th International Online Conference on Nanomaterials, 5–19 May 2023; Available online: https://iocn2023.sciforum.net.

Abstract: In this study, YCeO nanocomposites were efficaciously synthesized by the hydrothermal method in the company of sodium hydroxide as a reducing agent as well as cerium nitrate and yttrium nitrate as a precursor. Synthesis temperature and pressure, during hydrothermal reactions, show a critical role in governing the shape, size, oxygen vacancy attentiveness, and low-temperature reducibility in CeO_2-based nanocomposites. The lattice constants of the yttrium ceria nanocomposite also are contingent upon the attentiveness of hydroxide ions which primes to better morphology at low temperatures and pressure. XRD pattern of YCeO shows the Cubic structure of space group Fm3m having density 6.74 gm cm^{-3}, volume 157.81 × 10^6 pm^3, crystallite size 18.66 nm and lattice strain is 0.0041 and many more structural parameters were calculated. FE-SEM and AFM studies show the granular structure and surface roughness. Surface porosity and specific surface area were observed by BET, average nanoparticle size was analyzed by the analyzer, and optical properties were observed by FTIR and showing various chemical groups and UV-Visible with band gap 3.27 eV and absorbance at 256.58 nm lastly thermal stability of this nanoparticle was analyzed by TGA.

Keywords: cerium oxide; yttrium oxide; nanocomposite; hydrothermal; morphology

Citation: Srivastava, S.; Pandey, N.K. Low-Cost Hydrothermally Synthesized Multifunctional Rare Earth Metal Yttrium Cerium Oxide. *Mater. Proc.* **2023**, *5*, x. https://doi.org/10.3390/xxxxx

Published: 5 May 2023

1. Introduction

Rare earth metal oxides are very rousing materials due to their exclusive optical, electronic, magnetic, etc. [1]. All these chattels lead to many real-world applications such as Optics Communications, optical displays, efficient catalysis, UV shielding, and medical Diagnosis, industries [2]. Therefore, it primes extensive high-tech applications to occur because the quantum efficiency is too low [3]. In wide-ranging, all of these applications necessitate nanoparticles to have explicit possessions. Cerium oxide nanoparticles have advanced tremendously in the field of biomedical sciences, industrial, and many other fields, all of these applications have not only been verified to be obligatory for humans, but they are also playing a noteworthy role in the worldwide economic growth of many businesses. The studies done in this expanse have provided decisive evidence of the signs of progress and establishment. On the other hand, Yttrium oxide nanoparticles have many uses in the dominion of materials research, including coloring television picture tubes, flat panels, plasma displays, strong microwave filters, and many more. A critical starting point for the inorganic amalgamation of chemicals is yttrium oxide, which also has the capability to emanate red light a feature employed in fluorescent lighting. And the great application in X-ray and X-ray sensors that exploits ultrafast sensors and many more additional applications.

However, there are presently fewer reports on the investigation of novel CeO_2/Y_2O_3 composite materials with cubic structure and mesopores, which are intriguing scenarios for a variety of applications due to their massive surface area, stability, and low noxious-

ness. Several procedures have been working to create nanocomposites with the anticipated properties, together with co-precipitation [4], sol-gel [5], solvothermal [6], sono chemical [7], electrochemical approach [8], sputtering [9,10], arc-discharge [11], and solvothermal [7]. On bright of this, we designate the synthesis and properties of cerium/yttrium oxide nanoparticles made using the hydrothermal method, a straightforward technique for creating nanocrystals from aqueous solutions at low temperatures and high vapor pressures in an autoclave lined with Teflon further that XRD and FE-SEM, AFM, Nanoparticle Size Analyzer, FTIR, UV-Visible, BET, TGA were performed for a complete understanding of the structural and morphology.

2. Materials and Methods

In this present work, high-purity chemical reagents were of srl grade there after being used without further purification. We use Hydrothermal synthesis for the preparation of conflation of nanoparticles, a sufficient amount of 0.1 M Cerium (III) nitrate hexahydrate (Ce $(NO_3)_3 \cdot 6H_2O$) and 0.1 M Yttrium (III) nitrate hexahydrate ($Y(NO_3)_3 \cdot 6H_2O$ were dissolved in distilled water for 6 h to get the homogeneous solution. At the same time, 0.5 M of NaOH was dissolved in distilled water until it complete dissolve. Then NaOH was added dropwise slowly to the previous solution at room temperature until the pH becomes 10–11 with continuous stirring to attain a complete homogeneous solution. After that, the complete mixture was transferred into a 100 mL Teflon-lined autoclave and placed in an oven at 160 °C for 8 h. Then the autoclave was taken outside and allowed to cool at room temperature, we obtained a little pale-yellow precipitate was formed, which was kept in the oven at 100 °C for drying. Thus, the obtained powder was annealed at 550 °C then allowed to cool at room temperature, and powdered nanocomposite YCeO was formed, mixed with cerium/yttrium nanocomposites which are given in the following chemical Equations (1) and (2).

$$Ce(NO_3)_3(aq) + Y(NO_3)_3(aq) + 6NaOH \longrightarrow Ce(OH)_3(s) + Y(OH)_3(s) + 6NaNO_3(aq) \quad (1)$$

$$Ce(OH)_3(s) + 4Y(OH)_3(s) + O_2 \longrightarrow 4CeO_2(s) + 4Y_2O_3(s) + 12H_2O(L) \quad (2)$$

3. Result and Discussion

3.1. XRD Analysis

Powder X-ray diffraction, a non-destructive analytical technique for identifying the multiple crystalline phases of binary metal oxide nanocomposite, was used to examine the crystalline phase of the samples as prepared. Using a powder diffractometer and Cu-K radiations with a 2-theta range of 10°–80°, it is captured. The phases of cerium oxide or yttrium oxide were found among all the recorded peaks from the XRD pattern, and it is evident that all the diffraction peaks are precisely coincident with the cubic phase of binary metal oxide [15,16]. Additionally, it demonstrates the produced nanoparticles' excellent crystallinity and single phase of cubic fluorite crystal structure in the (Fm3m) space group. The X-ray diffraction was performed to obtain the crystal and phase structure of the Yttrium Cerium oxide that X-ray pattern was shown in Figure 1, different 2 θ peaks were 3 observed at 28.587, 33.128, 47.553, 56.427, 59.179, 69.524, 76.827 and 79.207 attributed to the (111), (200), (220), (311), (222), (400), (331) and (420) miller indices correspond to the cubic structure of YCeO. The crystal structure shown in Figure 2 was obtained from XRD data and was designed by Vista software. Here I can show the crystal structure of Cerium oxide, Yttrium oxide, and then the nanocomposite of Yttrium Cerium oxide crystal structure by combing both structures. After that, I'll show a single layer of Yttrium Cerium oxide for a better understanding of the atomic layer structural sites Lastly the multilayer cubical/slab structure of Yttrium Cerium oxide was also shown here to see and understand the surface structure then after a slab structure multi-layered structure was finally shown for a better understanding of the complete crystal structure which was

built after the composition of both nanomaterials. Different parameters were obtained such as volume density, space group, lattice/grain size, and many more calculated by refinement and different formulas as tabulated in Table 1, by different formulas.

The Williamson–Hall plot (β cosθ vs. sinθ) is attained from XRD results. As the laser effect increases, the slope of the Williamson–Hall plot increases. Due to strain toughening, the size of the diffraction peak increases as a result of the increase in lattice strain and the decrease in crystallite size. Crystal imperfections and distortion of strain-induced peak broadening are related by $\varepsilon \approx \beta s/\tan\theta$. Scherrer-equation follows a $1/\cos\theta$ dependence but not tanθ as the W-H method. Dependent on dissimilar θ positions the parting of size and strain broadening examination is done using Williamson and Hall, the graph shown in Figure 1 shows the WH plot which we calculated from the XRD analysis.

Table 1. Calculated structural parameters of YCeO crystal structure.

S. No	Calculated Parameters	YCeO
1.	Empirical Formula	$Ce_{0.80}O_{1.90}Y_{0.20}$
2.	Chemical Formula	$Y_{0.20}Ce_{0.80}O_{1.90}$
3.	Lattice system	Cubic
4.	Crystal system	Cubic
5.	Space group	Fm3m
6.	Space number	225
7.	a (Å)	5.4040
8.	b (Å)	5.4040
9.	c (Å)	5.4040
10.	α (°)	90
11.	β (°)	90
12.	γ (°)	90
13.	Density (gm cm^{-3})	6.74
14.	Volume (10^6) pm^3	157.81
15.	Z (no. of molecules)	4
16.	RIR (Reference intensity ratio)	13.60
17.	Crystallite (grain) size (nm)	18.66
18.	Lattice Strain	0.0041
19.	Dimensionality	3D
20.	Degree of Freedom	6
21.	R-Square (COD)	0.16363
22.	Adj. R-Square	0.02423

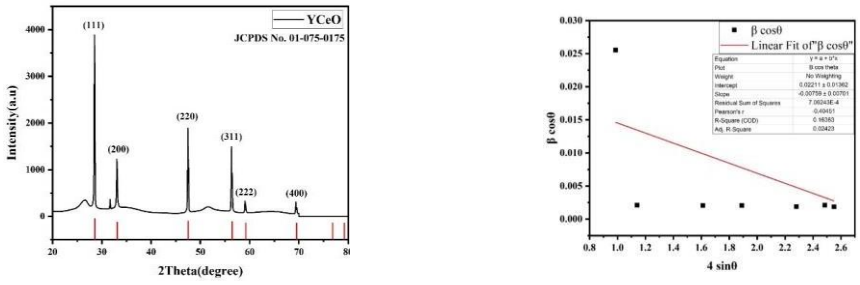

(**a**) (**b**)

Figure 1. Graph (**a**) shows the XRD pattern of YCeO with reference JCPDS no. and graph (**b**) shows the William Halson plot obtained from XRD data.

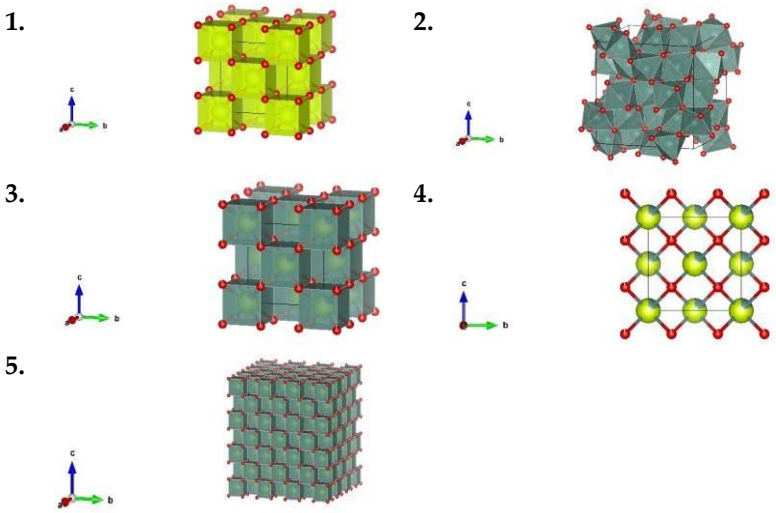

Figure 2. Different crystals of YCeO (number 1 is the structure of CeO_2, number 2 shows the structure of YO_3, number 3 shows the complete crystal structure of cubic YCeO [19], number 4 shows the single layer of YCeO, number 5 shows multilayer crystal cubic structure of YCeO.

3.2. FE-SEM Analysis

In examining the interactions between nanomaterials, the purity and shape of the nanoparticles are unquestionably essential elements. The two nanoparticles are therefore measured using a FESEM and the results are presented. Both nanoparticles generally showed the same morphology as fused and aggregated nanoparticles. Field Emission Scanning Electron Microscope was performed for a better understanding of the structure and morphology, Figure 3 shows the image taken from FE-SEM at 100 nm and shows the surface morphology and calculated its average particle size of 206.68 nm at particle distribution graph.

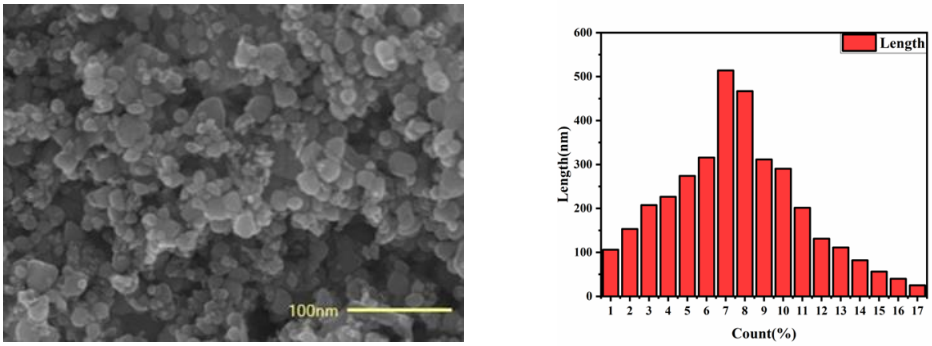

Figure 3. (**a**) shows the FE-SEM micrograph of YCeO under 100 nm and (**b**) shows the average particle distribution size which was calculated by the micrograph image FE-SEM.

3.3. AFM Analysis

For quantitatively determining the nanometric dimensional surface roughness and for seeing the surface nano-texture of the deposited film, atomic force microscopy examination is the best option. The surface of the as-grown YCeO films has a granular texture, as seen in the AFM images in Figure 4a,b, which is comparable to that seen in the SEM investigations. The crystallites are larger in the AFM images, though, because of tip convolution. The SEM photos show that the borders of the tiny spaces between the grains appear to be less crisp for the same reason. In contrast to the "hill" region, which is made up of numerous crystal-like structures that have certain orientations, the "valley" region

is comparatively smooth. As calculated its RMS (root mean square) roughness was 50.82 nm, mean roughness was 40.49 and Average became 126.1 nm.

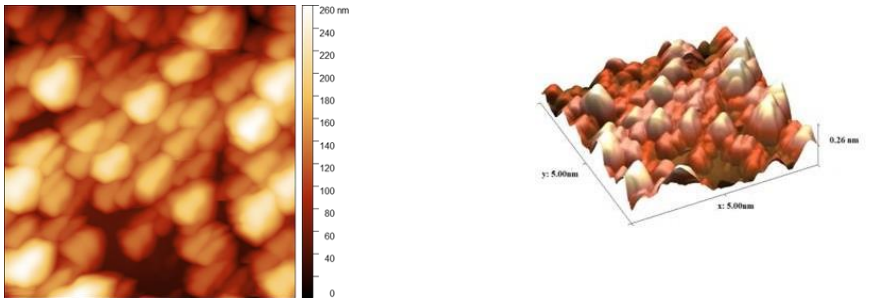

(**a**) (**b**)

Figure 4. (**a**) shows the observed AFM micrograph of yttrium cerium oxide nanoparticle in the nanometer range and (**b**) shows the 3D view of the AFM micrograph.

3.4. Nanoparticle Size Analyzer

The size of each particle as well as the size distribution range for a certain sample is determined using a nanoparticle size analyzer. In the study of nanoparticle characteristics and the interaction of cell materials, size distribution is a crucial and highly favorable feature. The size of the YCeO particles in deionized water is shown in Figure 5. According to the DLS measurement, the YCeO's average particle size was 690 nm in 100%. Those have a particle distribution peak from 359.09 to 1726.40 nm The increased particle size (found through DLS measurement) may be due to anticipated agglomerations and dynamic scattering of the nanoparticles in the dispersion medium [18].

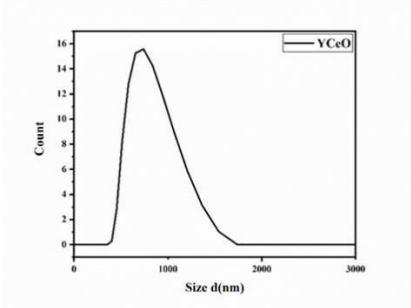

Figure 5. Graph of Nanoparticle size distribution.

3.5. FTIR Spectroscopy Analysis

To determine the chemical integrity of the tested nanoparticles, FTIR measurements were carried out. The spectra are shown in Figure 6 with wave numbers ranging from 400 to 4000 cm^{-1}. The O-H stretching vibration in OH groups is the cause of the large bandwidth that is specifically seen at 3000–3500 cm^{-1}, according to the details of the observation. The bands observed between 1250 and 1750 cm^{-1} are caused by the asymmetric stretching of the C-O band, which may result from the absorption of CO2 from the environment. The bands seen at about 750 cm^{-1} are attributed to the Y-O bond stretching vibration as closed with the wave number stated in the earlier investigation by Schwartz and Schwartz [13]. It can be shown from the FTIR analysis that the sample is a mixed composite of cerium and yttrium oxide. The lattice vibration modes of M-O and O-M-O correspond to the bands in the low-frequency range of 400 cm^{-1} to 1000 cm^{-1} (Ce, Y). The fact that the YO absorption bands are wider in Ce1/Y2 samples than they are in Ce2/Y1 samples suggests this [12].

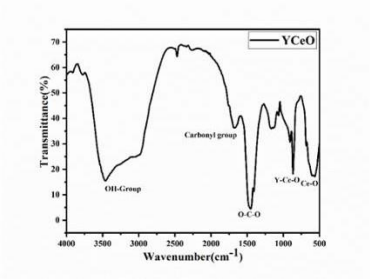

Figure 6. FTIR Spectra of yttrium cerium oxide nanocomposite.

3.6. UV-Visible Spectroscopy Analysis

Figure 7 illustrates the YCeO UV-Vis (250–900 nm) absorption spectrum. Around 256.58 nm in the UV area is where the absorption was discovered. Particle size distribution and flaws may be to blame for the gradual increase in absorbance and broadening of the absorbance peak. According to Equations (3) and (4) of Beer-relation, Lambert's absorption coefficient (α) can be calculated: where x is the cuvette's thickness, Io is the initial photon intensity, I is the instantaneous photon intensity,

$$I = I_o e^{-ax} \quad (3)$$

$$\alpha(\lambda) = [\ln (I_o/I)]/x = [\ln T/x] = 2.303A/x \quad (4)$$

The transition between extended states in the valence and conduction bands is what causes the greater value of the structure in the UV region (330–400 nm). Using Tauc's figure, the value of the optical energy band gap for YCeO was examined. To get the optical band gap, Tauc's relation from Equation (5) was employed (Eg) [14].

$$\alpha = [\alpha o(h\nu - Eg)^n]/h\nu \quad (5)$$

Here, the photon energy ($h\nu$), the absorbance coefficient (α), the characteristic parameter (αo), Planck's constant (h), and the power factor (n), are all defined. Depending on the nature of the transition, n may take on different values. Since the transition, in this case, is of the directly authorized kind, the value of n is taken to be ½ is what Eg for YCeO is calculated to be 3.27 eV

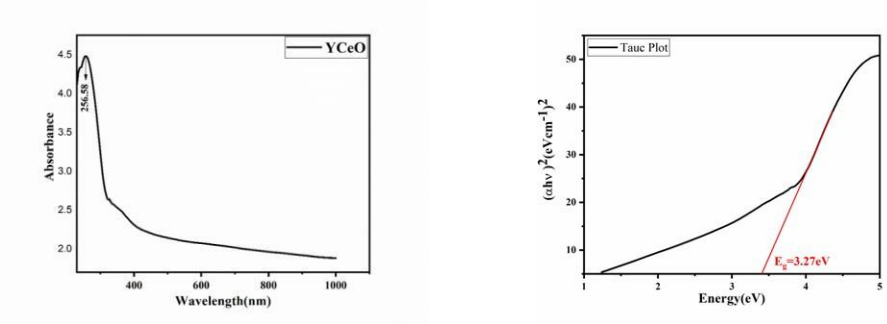

(**a**) (**b**)

Figure 7. (**a**) shows the UV-Visible Absorption spectra and (**b**) shows the band gap of yttrium cerium oxide nanocomposite.

3.7. TGA Analysis

To quantify the thickness of the coating on the nanoparticle's surface, thermogravimetric analysis (TGA) might be utilized. This estimate offers details on both chemical and physical events, including stage shifts, ingestion, adsorption, desorption, composition, purity, decomposition reactions, decomposition temperatures, and absorbed moisture content. Thermal analysis, in its broadest sense, refers to a method for determining the

temperature and time at which a substance undergoes physical changes when heated or cooled. TGA is a crucial tool for viewing particles at various temperatures since an object's temperature affects the mobility of its particles (the higher the temperature, the faster the particles must move to maintain stability). From the Figure 8 graph that 0.83% of the weight is lost at 200 °C and at last only 1.15% of the weight is lost up to 1000 °C, it can be shown that yttrium cerium oxide nanocomposite has better stability at high temperatures also.

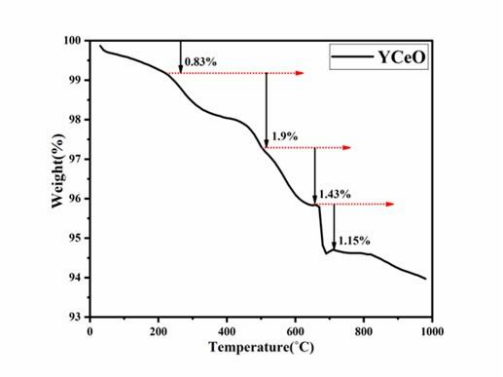

Figure 8. Fig shows the TGA graph observed of yttrium cerium oxide nanoparticles for thermal stability.

3.8. BET Analysis

Using the Brunauer-Emmett-Teller (BET) analytical physical characterization approach, solid materials' precise surface areas and porosity distributions are quantified. A wide variety of solid matrices, including monolithic materials and catalyst powders, can be used using this approach [17]. In this present work BET with Nitrogen dioxide at saturated pressure 101.54 [kPa] at a sample weight of 0.05 g with 9.792 slandered volume at an adsorption temperature of 77 k. We observed the volume of YCeO is 1.8573 cm^3/g, and the specific surface area was calculated as 8.084 m^2/g which is shown in the given graph Figure 9 shows the pore graph of the material shows its porosity, from this relative pressure or total pore volume was(p/p_o) was 0.090 cm^3/g, and the mean pore diameter calculated as 44.983 nm. Hence, it was observed that YCeO has a great specific surface area and porous material which proves that this material has to play a great and prominent role in many applications.

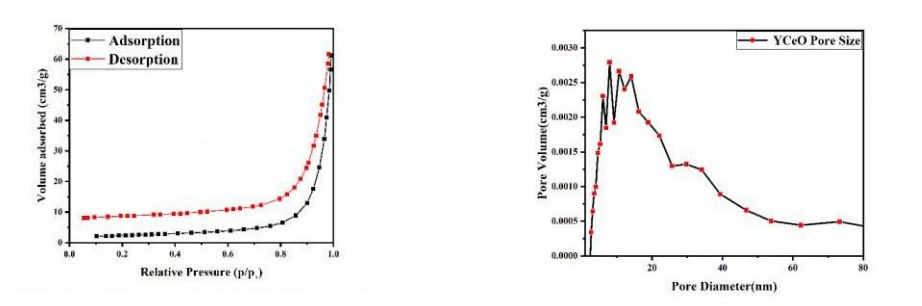

(**a**) (**b**)

Figure 9. (**a**) shows the adsorption and desorption of NO_2 and (**b**) shows the pore size of YCeO.

4. Conclusions

In this present work rare earth metal, Yttrium Cerium oxide was synthesized through one-step hydrothermal synthesis using yttrium nitrate (III) hexahydrate and cerium nitrate (III) hexahydrate as a starting precursor. XRD characterization was performed for un-

derstanding the structure of YCeO nanocomposite and found a well-shaped cubic structure and many more parameters calculated from Xpert Highscore and Fullprof software. For a complete analysis of the structural morphology, FE-SEM was performed, and the calculated average particle size of 206.68 nm. Further that AFM was performed for the surface roughness, and DLS measurement was performed to get an average particle size peak and the distribution was 690 nm and 359.09 to 1726.40 nm. FTIR confirmed the functional groups present, UV-Visible observed the wavelength of 256.68 nm and found the band gap of 3.27 eV, TGA confirm the nanocomposite stability up to 1000 °C and lastly, BET analyzes the specific surface area of YCeO was 8.084 m^2/g and mean pore diameter was 44.983 nm. This report purely focused on the structural and morphological property of Yttrium Cerium oxide nanocomposite and analyze that yttrium cerium oxide contains a high specific surface area, and average particle size which plays an important role in the adsorption process, heterogeneous catalysis, detection of molecules in a gas environment, biological application and many more. This low-cost technique synthesized YCeO nanocomposite has suitable for a wide range of applications such as sensors, industrial, automobiles, etc.

Author Contributions: For research articles Visualization, writing, graphics, characterization: S.S.; supervision, formal analysis, visualization: N.K.P. All authors have read and agreed to the published version of the manuscript.

Funding: This research received no external funding.

Acknowledgments: The authors would identical to prompt their gratitude to thank my supervisor or guide as well as our Head of Department, N.K. Pandey (University of Lucknow) for always supporting us. Secondly, I would like to thank Mohammad Abu Sazz (Banaras Hindu University) for helping me with the research synthesis Third I would like to thank Rajiv Prakash, Dean (IIT BHU) for helping me to use the hydrothermal technique. I would also thank to the CIF (Central instrument facility) of IIT BHU for helping in the XRD, TGA, BET, BHU for using AFM, Thanks for BSIP Lucknow for FE-SEM characterization, and last the chemistry department, University of Lucknow for UV-Visible and FTIR facility.

Conflicts of Interest: The authors declare no conflict of interest.

References

1. Zhang, C.; Zhang, X.; Wang, Y.; Xie, S.; Liu, Y.; Lu, X.; Tong, Y. Facile electrochemical synthesis of CeO_2 hierarchical nanorods and nanowire with excellent photocatalytic activities. *New J. Chem.* **2014**, *38*, 2581–2586.
2. Goharshadi, E.K.; Samiee, S.; Nancarrow, P. Fabrication of cerium oxide nanoparticles: Characterization and optical properties. *J. Colloid Interface Sci.* **2011**, *356*, 473–480.
3. Kaviyarasu, K.; Manikandan, E.; Nuru, Z.Y.; Maaza, M. Investigation on the structural properties of CeO_2 nanofibers via CTAB surfactant. *Mater. Lett.* **2015**, *160*, 61–63.
4. Ameta, K.L.; Papnai, N.; Ameta, R. Photocatalytic Degradation of Malachite Green Using Nano-sized cerium-iron Oxide. *Orbital Electron. J. Chem.* **2014**, *6*, 4–19.
5. Magdalene, C.M.; Kaviyarasu, K.; Vijaya, J.J.; Jayakumar, C.; Maaza, M.; Jeyaraj, B. Photocatalytic degradation effect of malachite green and catalytic hydrogenation by UV–illuminated CeO_2/CdO multilayered nanoplatelet arrays: Investigation of antifungal and antimicrobial activities. *J. Photochem. Photobiol. B Biol.* **2017**, *169*, 110–123.
6. Gu, S.; Chen, Y.; Yuan, X.; Wang, H.; Chen, X.; Liu, Y.; Jiang, Q.; Wu, Z.; Zeng, G. Facile synthesis of CeO_2 nanoparticles sensitized CdS nanorods photocatalyst with improved visible-light photocatalytic degradation of Rhodamine B. *RSC Adv.* **2015**, *5*, 79556–79564. https://doi.org/10.1039/C5RA16114B.
7. Askarinejad, A.; Morsali, A. Syntheses and characterization of $CdCO_3$ and CdO nanoparticles by using a sonochemical method. *Mater. Lett.* **2008**, *62*, 478–482.
8. Zhao, M.; Li, H.; Shen, X.P.; Ji, Z.Y.; Xu, K.Q. Facile electrochemical synthesis of CeO_2@Ag@CdS nanotube arrays with enhanced photoelectrochemically water splitting performance. *Dalton Trans.* **2015**, *44*, 19935–19941. https://doi.org/10.1039/C5DT03661E.
9. Couture, P.; Williams, G.V.M.; Kennedy, J.; Leveneur, J.; Murmu, P.P.; Chong, S.V.; Rubanov, S. Multiferroic nanocrystalline $BiFeO_3$ and $BiCrO_3$ thin films prepared by ion beam sputtering. *Int. J. Nanotechnol.* **2017**, *14*, 56–65.
10. Couture, P.; Williams, G.V.M.; Kennedy, J.; Leveneur, J.; Murmu, P.P.; Chong, S.V.; Rubanov, S. Nanocrystalline multiferroic $BiFeO_3$ thin films made by room temperature sputtering and thermal annealing, and formation of an iron oxide-induced exchange bias. *J. Alloys Compd.* **2017**, *695*, 3061–3068.
11. Kennedy, J.; Fang, F.; Futter, J.; Leveneur, J.; Murmu, P.P.; Panin, G.N.; Kang, T.W.; Manikandan, E. Synthesis and enhanced field emission of zinc oxide incorporated carbon nanotubes. *Diam. Relat. Mater.* **2017**, *71*, 79–84.

12. Kaviyarasu, K.; Manikandan, E.; Nuru, Z.Y.; Maaza, M. Investigation on the structural properties of CeO_2 nanofibers via CTAB surfactant. *Mater. Lett.* **2015**, *160*, 61–63.
13. Traina, C.A.; Schwartz, J. Surface modification of Y_2O_3 nanoparticles. *Langmuir* **2007**, *23*, 9158–9916.
14. Verma, A.; Chaudhary, P.; Tripathi, R.K.; Yadav, B.C. Transient photodetection studies on 2D ZnO nanostructures prepared by simple organic-solvent assisted route. *Sens. Actuators A Phy.* **2021**, *321*, 112600.
15. Porqueras; Pearson, C.; Corbella, C.; Vives, M.; Pinyol, A.; Bertran, E. Characteristics of e-beam deposited electrochromic CeO_2 thin films. *Solid State Ion.* **2003**, *165*, 131–137.
16. Zhao, S.; Li, J.; Wang, L.; Wang, X. Degradation of Rhodamine B and Safranin-T by MoO_3:CeO_2 Nanofibers and Air Using a Continuous Mode. *Clean-Soil Air Water* **2010**, *38*, 268–274.
17. Hassellöv, M.; Readman, J.W.; Ranville, J.F.; Tiede, K. Nanoparticle analysis and characterization methodologies in environmental risk assessment of engineered nanoparticles. *Ecotoxicology* **2008**, *17*, 344–361. https://doi.org/10.1007/s10646-008-0225-x.
18. Mahapatra, C.; Singh, R.K.; Lee, J.H.; Jung, J.; Hyun, J.K.; Kim, H.W. Nano shape varied cerium oxide nanomaterials rescue human dental stem cells from oxidative insult through intracellular or extracellular actions. *Acta Biomater.* **2017**, *50*, 142–153.
19. Brauer, G.; Gradinger, H. Ueber heterotype Mischphasen bei Seltenerdoxyden. I. *Z. Anorg. Allg. Chem.* **1954**, *276*, 209–226.